

Calculation of dynamic stress intensity factors and T-stress using an improved SBFEM

Xinran Tian¹, Chengbin Du^{*1}, Shangqiu Dai¹ and Denghong Chen²

¹Department of Engineering Mechanics, Hohai University, Nanjing 210098, China

²College of Civil Engineering and Architecture, China Three Gorges University, Yichang 443002, China

(Received October 28, 2017, Revised March 7, 2018, Accepted March 11, 2018)

Abstract. The scaled boundary finite element method is extended to evaluate the dynamic stress intensity factors and T-stress with a numerical procedure based on the improved continued-fraction. The improved continued-fraction approach for the dynamic stiffness matrix is introduced to represent the inertial effect at high frequencies, which leads to numerically better conditioned matrices. After separating the singular stress term from other high order terms, the internal displacements can be obtained by numerical integration and no mesh refinement is needed around the crack tip. The condition numbers of coefficient matrix of the improved method are much smaller than that of the original method, which shows that the improved algorithm can obtain well-conditioned coefficient matrices, and the efficiency of the solution process and its stability can be significantly improved. Several numerical examples are presented to demonstrate the increased robustness and efficiency of the proposed method in both homogeneous and bimaterial crack problems.

Keywords: scaled boundary finite element method; stress intensity factors; T-stress; improved continued-fractions

1. Introduction

In the linear elastic fracture mechanics (LEFM), dynamic stress intensity factors (DSIFs) are the most important parameters for predicting the initiation and propagation of cracks in structures subjected to dynamic loadings. Both analytical methods and numerical methods, such as the finite difference method (FDM), the finite element method (FEM), the boundary element method (BEM) and two more recent numerical approaches: the extended FE method (XFEM) and meshfree methods, have been widely applied to calculate the DSIFs. In most of these existing methods, computing the stress field around the crack tip and extracting the singular stress from the stress field are two key tasks of the dynamic fracture problems.

In general, the analytical methods are only available for problems with simple geometries and loading conditions and the solutions are usually very complicated. Therefore, numerical methods play significant roles in understanding different behaviors of materials and structures that experience dynamic loads. The FDM (Chen 1975) is the first numerical method applied to calculate the DSIFs. However, it has been rarely used to solve the dynamic fracture problems due to the difficulty in modeling complex geometries. The FEM, as one of the most popular numerical methods in engineering problems, soon became the primary choice for calculating DSIFs, because it can handle complex geometries and material properties conveniently. Various methods have been proposed to evaluate DSIFs, i.e., the path independent integral method (Rice 1967), the

virtual crack extension method (Réthoré *et al.* 2004), the quarter-point element (Barsoum 1977, Murti and Valliappan 1986) and hybrid crack element (Xiao *et al.* 2004). However, FEM and all above the mentioned methods rely on a conforming mesh and the mesh around a crack tip should be refined to accurately represent the stress singularities, which are inefficient to deal with crack problems.

In an effort to overcome the limitations of FEM, XFEM and meshfree methods were introduced. In XFEM, the discontinuities around the crack tip are represented by proposing enrichment functions to cover or be closer to the exact solution (Belytschko *et al.* 2003). Since the mesh is not required to match the geometry after combining it with the level set functions, XFEM has been treated as a versatile tool to solve the discontinuous problems. For example, Legrain *et al.* (2011) applied XFEM to determine the fracture properties of different composite structures and Jiang *et al.* (2014) studied the DSIFs for structures containing multiple discontinuities by four types of enrichment functions. Jiang (Jiang *et al.* 2014) also studied the effect of the containing multiple discontinuities (voids, inclusions, and cracks) in structures by XFEM. In meshfree methods, the conforming mesh is not required as the discontinuities evolve which makes it more straightforward in crack problems (Rabczuk and Belytschko 2006, Rabczuk *et al.* 2008, Rabczuk *et al.* 2009, Jamal-Omidi *et al.* 2014). Domain integrals (Yau *et al.* 1980) are usually used to calculate SIFs with meshfree methods. Like XFEM, the enrichment functions can also be introduced to improve the accuracy of DSIFs (Rao and Rahman 2004). Although the two methods are robust, they still suffer from certain difficulties, such as the requirement of fine meshes and fine nodal distributions separate, and continuous research is

*Corresponding author, Professor
E-mail: cbdu@hhu.edu.cn

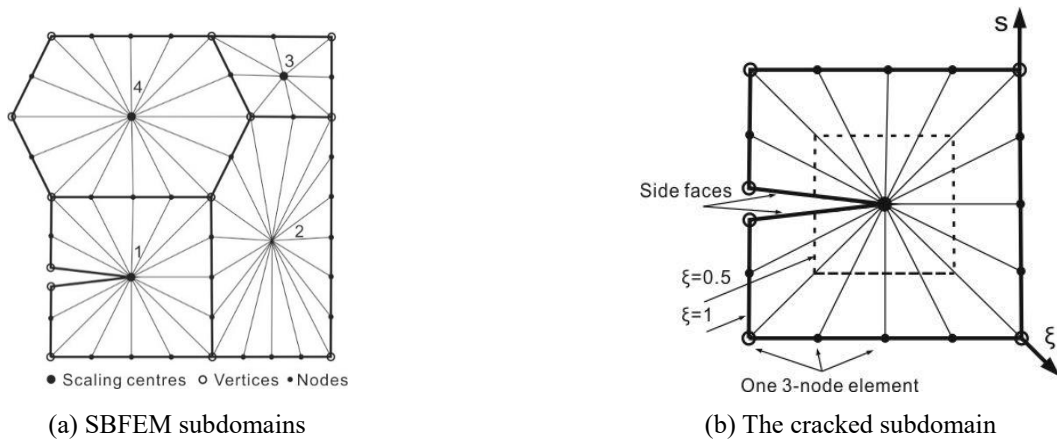


Fig. 1 Concept of scaled boundary finite element method

carried out to improve the capability of the methods.

The BEM is a competitive alternative to FEM in computing DSIFs because only the boundaries are necessary to discretized and the representation of cracks is much simpler than the FEM. However, its applicability is limited by the requirement of fundamental solutions. Enormous research effort has been proposed to improve the existing BEM approach, i.e., the dual boundary element method (Portela *et al.* 1993), the dual reciprocity method (Fedelinski 2010) and the enriched BEM methods (Simpson and Trevelyan 2011).

The scaled boundary finite element method (SBFEM), as a semi-analytical method developed by Song and Wolf (1997, 2002) in the 1990s, is highly efficient in solving problems involving singularities, because the stress singularity can be represented analytically without enrichment functions or analytical asymptotic expansions and only the boundary is discretized as the BEM. It has been well demonstrated by studies calculating static SIFs for isotropic materials (Chidgzezy and Deeks 2005, Li and Tong 2015), anisotropic materials (Song and Wolf 2002), functionally graded materials (Chiong *et al.* 2014) and piezoelectric composites (Li *et al.* 2015). Crack propagation is modeled for static problems with several simple remeshing methods, such as polygon elements (Dai *et al.* 2014, Ooi *et al.* 2016, Chen and Dai 2017), quadtree meshes (Ooi *et al.* 2015, Ooi *et al.* 2017, Saputra *et al.* 2017) and a non-matching method (Yang *et al.* 2015). According to these attributes, the SBFEM has also been exploited in coupling with BEM (Chidgzezy *et al.* 2008) or XFEM (Natarajan and Song 2013, Natarajan *et al.* 2014) for calculating parameters in static fracture problems.

For dynamic fracture mechanics analyses, a super-element, represented by the static stiffness matrix and mass matrix, is proposed by Song (2004b). The dynamic crack propagation has been modeled based on this kind of elements (Ooi and Yang 2011, Ooi *et al.* 2013). In order to represent the highest frequency component, the size of the super-element should be small enough, which may lead to considerable effort in mesh generation and computational cost in each step. Instead of this super-element, a frequency domain method to calculate DSIFs for homogenous materials (Yang *et al.* 2007) and bimaterial interface

problems (Yang and Deeks 2008) are presented by Yang, but it is not easily amendable to a time domain crack propagation. Recently, the dynamic analysis of isotropic and anisotropic materials has been performed efficiently with a novel solution procedure, known as the continued-fraction algorithm, in both frequency and time domain (Song *et al.* 2010b, Song and Vrcelj 2008), in which the high frequency responses of structures are represented by the high-order terms (Song 2009). However, the method may break down when a system requires a large number of DOFs and approximations of high-order expansions (Chen *et al.* 2014). In such cases, the improved continued-fraction of bounded domain (Chen *et al.* 2014) is more suitable for dynamic fracture problems.

In this paper, a numerical procedure based on the improved continued-fraction is developed to extract the dynamic stress intensity factors and T-stress using the scaled boundary finite element method. The dynamic properties of the structures are represented by the high-order expansions of stiffness and mass matrices. A differential equation containing the coefficients of improved continued-fraction is presented to remove the stress singularity analytically. The dynamic fracture parameters are extracted directly in the time domain according to the definition of the generalized stress intensity factors (Song *et al.* 2010a).

This paper is organized as follows. In Section 2, the scaled boundary finite element method and the solution procedure based on the improved continued-fraction are summarized. In Section 3, a numerical procedure to calculate the internal displacement and stress is proposed. In Section 4, the dynamic stress intensity factors and T-stress are extracted with the definition of the generalized stress intensity factors. In Section 5, several examples are presented to demonstrate the efficiency of the proposed method. In Section 6, the major conclusions are summarized.

2. The scaled boundary finite element method

The derivation of the scaled boundary finite element method for elastodynamics is presented by Song and Wolf

(1997, 2000). The solution procedure for dynamic problems with the improved continued fraction is detailed by Chen *et al.* (2014).

The basic concept of the SBFEM is illustrated in Fig. 1(a) and (b). As shown in Fig. 1(a), a typical domain with irregular shape can be divided into four subdomains, in which subdomain 1 contains a crack (named the cracked subdomain). A so-called scaling center is chosen in each subdomain from which all of its boundaries are visible. Only the boundaries of the subdomains are necessary to discretize with different kinds of line elements, i.e. the three-node line element (shown in Fig. 1(a)). The details of the cracked subdomain are shown in Fig. 1(b). For the cracked subdomain, the scaling center is selected at the crack tip and the two straight lines passing through the scaling center are not discretized. Without losing generality, the coordinates of the nodes on the boundaries are uniquely defined by a local coordinate system (ξ, s) whose origin is at the scaling center. One circumferentially similar curve with $\xi=0.5$ is also shown in Fig. 1(b).

The key governing equilibrium equations of SBFEM for elastodynamics are expressed as follows (Song and Wolf 1997, Wolf and Song 2000)

$$[E^0] \xi^2 \{u(\xi)\}_{,\xi\xi} + ([E^0] - [E^1] + [E^1]^T) \xi \{u(\xi)\}_{,\xi} - [E^2] \{u(\xi)\} + (\omega\xi)^2 [M^0] \{u(\xi)\} = 0 \quad (1)$$

$$\{q(\xi)\} = [E^0] \xi \{u(\xi)\}_{,\xi} + [E^1]^T \{u(\xi)\} \quad (2)$$

where ω is the excitation frequency. The coefficient matrices $[E^0]$, $[E^1]$, $[E^2]$ and $[M^0]$ are obtained by assembling the element coefficient matrices as in the finite element method. $\{u(\xi)\}$ and $\{q(\xi)\}$ are the nodal displacements and internal nodal force functions, respectively.

The dynamic stiffness matrix of a bounded domain $[S(\omega, \xi)]$ is defined as

$$\{q(\xi)\} = [S(\omega, \xi)] \{u(\xi)\} \quad (3)$$

Eliminating $\{u(\xi)\}$ and $\{q(\xi)\}$ from Eqs. (1), (2) and (3) and changing the independent variable to

$$x = -(\omega\xi)^2 \quad (4)$$

The so-called SBFEM equation for the dynamic stiffness is rewritten as

$$([S(x)] - [E^1])[E^0]^{-1}([S(x)] - [E^1]^T) - [E^2] + 2x[S(x)]_{,x} - x[M^0] = 0 \quad (5)$$

The solution of the dynamic stiffness $[S(x)]$ can be expressed as the sum of a constant term $[K]$, a linear term $x[M]$ and a higher order residual term $-x^2[R^{(1)}(x)]$

$$[S(x)] = [K] + x[M] - x^2[R^{(1)}(x)] \quad (6)$$

where the first two terms $[K]$ and $[M]$ are the static stiffness and mass matrices respectively and represent the low

frequency expansion of the structure. $[R^{(1)}(x)]$, including the high-order terms of the continued fraction solution, represents the high frequency response of the structure. Substituting Eq. (6) into Eq. (5) yields

$$([K] - [E^1] + x[M] - x^2[R^{(1)}(x)])[E^0]^{-1}([K] - [E^1]^T + x[M] - x^2[R^{(1)}(x)]) + 2x([M] - 2x[R^{(1)}(x)] - x^2[R^{(1)}(x)]_{,x}) - [E^2] - x[M^0] = 0 \quad (7)$$

In the next step, arranging Eq. (7) in ascending orders of powers of x and setting each term equal to zero individually. The constant term is an algebraic Riccati equation for calculating the static stiffness matrix.

$$([K] - [E^1])[E^0]^{-1}([K] - [E^1]^T) - [E^2] = 0 \quad (8)$$

The solution procedure of Eq. (8) is described in detail by Song (2004b), where the real Schur decomposition of a Hamiltonian matrix is performed as follows

$$\begin{bmatrix} [E^0]^{-1}[E^1]^T & -[E^0]^{-1} \\ -[E^2] + [E^1][E^0]^{-1}[E^1]^T & -[E^1][E^0]^{-1} \end{bmatrix} \begin{bmatrix} V_{11} & V_{12} \\ V_{21} & V_{22} \end{bmatrix} = \begin{bmatrix} V_{11} & V_{12} \\ V_{21} & V_{22} \end{bmatrix} \begin{bmatrix} S_{11} & S_{12} \\ 0 & S_{22} \end{bmatrix} \quad (9)$$

The real Schur form matrix $[S]$ is a quasi-upper triangular matrix consisting of 1×1 blocks or 2×2 blocks on the diagonal $[V]$ is a transformation matrix. $[S]$ and $[V]$ are arranged in such a way that the real parts of the eigenvalues of $[S_{11}]$ are non-positive and $[V_{11}]$ contains the displacement modes corresponding to the eigenvalues.

Then the semi-positive definite static stiffness matrix $[K]$ can be obtained as

$$[K] = [V_{21}][V_{11}]^{-1} \quad (10)$$

To express the stress intensity factors and T-stress conveniently, $[S_{11}]$ is block diagonalized into

$$[S_{11}] = \text{diag}([S_{n1}], -[I], [S^{(s)}], 0) \quad (11)$$

and $[V_{11}]$ is partitioned conformably as

$$[V_{11}] = [[\psi_{n1}], [\psi^{(t)}], [\psi^{(s)}], [\psi^{(r)}]] \quad (12)$$

where the zero eigenvalues and $[\psi^{(r)}]$ describe the translational rigid body motions. The real parts of the eigenvalues in $[S^{(s)}]$ are between -1 and 0, which represent the singular stress terms with $[\psi^{(s)}]$. The T-stress and rotational rigid body motion are represented by $-[I]$ and $[\psi^{(t)}]$. The remaining diagonal blocks and displacement modes are grouped and denoted as $[S_{n1}]$ and $[\psi_{n1}]$ respectively. The real parts of the eigenvalues in $[S_{n1}]$ are all smaller than -1, which do not contribute to the singular stress.

The linear term of Eq. (7) is a Lyapunov equation for the mass matrix $[M]$

$$\begin{aligned} & ([K] - [E^1])[E^0]^{-1}[M] + [M][E^0]^{-1}([K] - [E^1])^T \\ & + 2[M] - [M^0] = 0 \end{aligned} \quad (13)$$

Its solution is obtained in Song and Wolf (1997) as

$$[M] = [V_{11}]^{-T}[m][V_{11}]^{-1} \quad (14)$$

where the matrix $[m]$ is the solution of the Lyapunov equation

$$\begin{aligned} & ([I] - [S_{11}]^T)[m] + [m]([I] - [S_{11}]) \\ & = [V_{11}]^T[M^0][V_{11}]^T \end{aligned} \quad (15)$$

The remaining part of Eq. (7) is an equation for the unknown residual $\{R^{(i)}(x)\}$, which is decomposed as

$$[R^{(i)}(x)] = [X^{(i)}][S^{(i)}(x)]^{-1}[X^{(i)}]^T \quad (16)$$

In Eq. (16), $[X^{(i)}]$ is an additional yet undetermined scaling factor which can lead to well-posed coefficient matrixes (Chen *et al.* 2014). The term $[S^{(i)}(x)]$ is an unknown function of x . Analogous to the dynamic stiffness matrix $[S(x)]$, it can be expanded into a constant term $[S_0^{(i)}]$, a linear term $x[S_1^{(i)}]$ and a higher order residual term $-x^2[R^{(i+1)}(x)]$

$$[S^{(i)}(x)] = [S_0^{(i)}] + x[S_1^{(i)}] - x^2[R^{(i+1)}(x)] \quad (17)$$

The equation for $[S^{(i)}(x)]$ is represented as the case $i = 1$ of the following equation

$$\begin{aligned} & [S^{(i)}(x)][c^{(i)}][S^{(i)}(x)] - [S^{(i)}(x)][b_0^{(i)}]^T \\ & - [b_0^{(i)}][S^{(i)}(x)] - x[S^{(i)}(x)][b_1^{(i)}]^T - x[b_1^{(i)}][S^{(i)}(x)] \\ & + 2x[S^{(i)}(x)]_{,x} + x^2[a^{(i)}] = 0 \end{aligned} \quad (18)$$

with the coefficient matrices defined as

$$[a^{(1)}] = [X^{(1)}]^T[E^0]^{-1}[X^{(1)}] \quad (19a)$$

$$[b_0^{(1)}] = [X^{(1)}]^T[E^0]^{-1}([K] - [E^1])^T[X^{(1)}]^{-T} - 2[I] \quad (19b)$$

$$[b_1^{(1)}] = [X^{(1)}]^T[E^0]^{-1}[M][X^{(1)}]^{-T} \quad (19c)$$

$$[c^{(1)}] = [X^{(1)}]^{-1}[M][E^0]^{-1}[M][X^{(1)}]^{-T} \quad (19d)$$

Substituting Eq. (17) into Eq. (18) leads to equations for $[S_0^{(i)}]$, $[S_1^{(i)}]$ and $[S^{(i+1)}(x)]$. The equation for $[S_0^{(i)}]$ and $[S_1^{(i)}]$ are two Lyapunov equations and represented as

$$[S_0^{(i)}]^{-1}[b_0^{(i)}] + [b_0^{(i)}]^T[S_0^{(i)}]^{-1} = [c^{(i)}] \quad (20)$$

$$\begin{aligned} & (-[b_0^{(i)}] + [S_0^{(i)}][c^{(i)}])[S_1^{(i)}] + [S_1^{(i)}](-[b_0^{(i)}]^T \\ & + [c^{(i)}][S_0^{(i)}]) + 2[S_1^{(i)}] \\ & = [b_1^{(i)}][S_0^{(i)}] + [S_0^{(i)}][b_1^{(i)}]^T \end{aligned} \quad (21)$$

It can be seen from Eqs. (20) and (21) that the coefficients $[S_0^{(i)}]$ and $[S_1^{(i)}]$ will be different from those calculated using the technique proposed in Song (2009) due to the modified definition of the coefficients $[a^{(i)}]$, $[b_0^{(i)}]$, $[b_1^{(i)}]$ and $[c^{(i)}]$ including the scaling factor $[X^{(i)}]$.

The equation for $[S^{(i+1)}(x)]$ is expressed as the $(i + 1)$ th case of Eq. (18)

$$\begin{aligned} & [S^{(i+1)}(x)][c^{(i+1)}][S^{(i+1)}(x)] - [S^{(i+1)}(x)][b_0^{(i+1)}]^T \\ & - [b_0^{(i+1)}][S^{(i+1)}(x)] - x[S^{(i+1)}(x)][b_1^{(i+1)}]^T \\ & - x[b_1^{(i+1)}][S^{(i+1)}(x)] + 2x[S^{(i+1)}(x)]_{,x} + x^2[a^{(i+1)}] = 0 \end{aligned} \quad (22)$$

with the coefficient matrices defined as

$$[a^{(i+1)}] = [X^{(i+1)}]^T[c^{(i)}][X^{(i+1)}] \quad (23a)$$

$$\begin{aligned} [b_0^{(i+1)}] & = [X^{(i+1)}]^T(2[I] - [b_0^{(i)}]^T \\ & + [c^{(i)}][S_0^{(i)}][X^{(i+1)}]^{-T}) \end{aligned} \quad (23b)$$

$$[b_1^{(i+1)}] = [X^{(i+1)}]^T(-[b_1^{(i)}]^T + [c^{(i)}][S_1^{(i)}])[X^{(i+1)}]^{-T} \quad (23c)$$

$$\begin{aligned} [c^{(i+1)}] & = [X^{(i+1)}]^{-1}([a^{(i)}] - [b_1^{(i)}][S_1^{(i)}] - [S_1^{(i)}][b_1^{(i)}]^T \\ & + [S_1^{(i)}][c^{(i)}][S_1^{(i)}])[X^{(i+1)}]^{-T} \end{aligned} \quad (23d)$$

The same strategy for solving Eq. (18) is applied to Eq. (22) again. If the coefficients $[X^{(i)}]$ are known, the matrices $[a^{(1)}]$, $[b_0^{(1)}]$, $[b_1^{(1)}]$ and $[c^{(1)}]$ can be calculated using Eq. (19). The coefficients $[a^{(i)}]$, $[b_0^{(i)}]$, $[b_1^{(i)}]$ and $[c^{(i)}]$ for $i \geq 2$ follow subsequently from updating using Eq. (23). The recursive procedure is terminated when $i = M_{cf}$ (the order of the continued fraction). This corresponds to the assumption the residual of order $M_{cf} + 1$ equaling to zero.

The final step of the improved continued fraction solution is to determine the coefficients $[X^{(i)}]$. According to the method in Chen *et al.* (2014), the LDL^T decomposition is applied to the coefficient $[c^{(i)}]$ in Eqs. (18) and (22)

$$\begin{aligned} [c^{(i)}] & = [X^{(i)}]^{-1}[\tilde{c}^{(i)}][X^{(i)}]^{-T}; \\ [\tilde{c}^{(i)}] & = [L^{(i)}][D^{(i)}][L^{(i)}]^T \end{aligned} \quad (24)$$

The coefficient $[X^{(i)}]$ is chosen as the lower triangular matrix $[L^{(i)}]$

$$[X^{(i)}] = [L^{(i)}] \tag{25}$$

where $[L^{(i)}]$ can be normalized such that the absolute value of the diagonal entries is one.

Using the improved continued fraction solution, the force-displacement relationship (Eq. (2)) then can be expressed as an equation of motion in the frequency domain and time domain.

$$([K_b] - (\omega\xi)^2)[M_b]\{Z(\xi)\} = \{F(\xi)\} \tag{26a}$$

$$[K_b]\{Z(\xi)\} + \xi^2[M_b]\{\ddot{Z}(\xi)\} = \{F(\xi)\} \tag{26b}$$

with the coefficient matrices expressed as

$$[K_b] = \text{diag}([K], [S_0^{(1)}], [S_0^{(2)}], \dots, [S_0^{(M_{cf}-1)}], [S_0^{(M_{cf})}]) \tag{27a}$$

$$[M_b] = \begin{bmatrix} [M] & -[X^{(1)}] & 0 & \dots & 0 & 0 \\ -[X^{(1)T}] & [S_1^{(1)}] & -[X^{(2)}] & \dots & 0 & 0 \\ 0 & -[X^{(2)T}] & [S_1^{(2)}] & \dots & 0 & 0 \\ \vdots & \vdots & \vdots & \ddots & -[X^{(M_{cf}-1)}] & 0 \\ 0 & 0 & 0 & -[X^{(M_{cf}-1)T}] & [S_1^{(M_{cf}-1)}] & -[X^{(M_{cf})}] \\ 0 & 0 & 0 & 0 & -[X^{(M_{cf})T}] & [S_1^{(M_{cf})}] \end{bmatrix} \tag{27b}$$

$$\{Z(\xi)\} = \begin{Bmatrix} \{u(\xi)\} \\ \{u^{(1)}(\xi)\} \\ \{u^{(2)}(\xi)\} \\ \vdots \\ \{u^{(M_{cf}-1)}(\xi)\} \\ \{u^{(M_{cf})}(\xi)\} \end{Bmatrix}, \quad \{F(\xi)\} = \begin{Bmatrix} \{q(\xi)\} \\ 0 \\ 0 \\ \vdots \\ 0 \\ 0 \end{Bmatrix} \tag{27c}$$

The matrices $[K_b]$ and $[M_b]$ are symmetric and sparse. If using the technique proposed in Song (2009), all-diagonal blocks in Eq. (27b) will be a unit matrix $[I]$, whereas the block-diagonal terms may strongly differ in magnitude. The example given in Song (2009) reveals that, in particular, the coefficients $[S_0^{(i)}]$ increase in magnitude along with the order of continued fraction increasing. Ultimately, the strong differences in magnitude between the terms of the identity matrix on the off block diagonal and the coefficients $[S_0^{(i)}]$ may reduce the computational efficiency and even lead to ill-conditioning of high order mass and stiffness matrices. The numerical examples presented in Section 5 will show that the scaling factors $[X^{(i)}]$ will lead to numerically better conditioned matrices $[S_0^{(i)}]$ and it will be more significant in the solution procedures for calculating fracture parameters.

3. Calculating the internal displacements and stresses

After solving the equation of motion of the global system, the nodal displacements and auxiliary variables at the boundary of each subdomain are obtained directly at discrete frequencies or time stations. Then all the displacements at the boundary can be determined based on the element connectivity as in the FEM. As to the internal displacements and stresses, the solution procedure for the static problems cannot be applied to the dynamic problems directly, because the high frequency components of the inertial force should be considered. In the following section, the procedure for extracting the internal displacements in the time domain with the improved continued fraction is proposed.

3.1 Asymptotic solution of internal displacements and stresses

The asymptotic solution for the displacement field is expressed in Song and Vrcelj (2008) as

$$\{u(\xi)\} = [V_{11}]\xi^{-[S_{11}]} \{c\} + O(\xi^2) \tag{28}$$

where $\{c\}$ are the integration constants which depend on the boundary conditions. $O(\xi^2)$ is a high order term that tends to zero with the same rate of ξ^{2n} and it contains the effect of the inertial force at high frequency. Substituting the matrix $[S_{11}]$ in Eq. (11) and $[V_{11}]$ in Eq. (12) into Eq. (28) leads to

$$\begin{aligned} \{u(\xi)\} &= [\psi^{(r)}]\{c^{(r)}\} + [\psi^{(s)}]\xi^{-[S^{(s)}]}\{c^{(s)}\} \\ &\quad + [\psi^{(T)}]\xi\{c^{(T)}\} + [\psi_{n1}]\xi^{-[S_{n1}]}\{c_{n1}\} \\ &\quad + O(\xi^2) \end{aligned} \tag{29}$$

And its derivative $\{u(\xi)\}_{,\xi}$ is expressed as

$$\begin{aligned} \{u(\xi)\}_{,\xi} &= -[\psi^{(s)}][S^{(s)}]\xi^{-[S^{(s)}]-[I]}\{c^{(s)}\} \\ &\quad + [\psi^{(T)}]\{c^{(T)}\} - [\psi_{n1}][S_{n1}]\xi^{-[S_{n1}]-[I]}\{c_{n1}\} \\ &\quad + O(\xi) \end{aligned} \tag{30}$$

where the integration constants $\{c\}$ are partitioned conformably as

$$\{c\} = \left\{ \left\{ c^{(r)} \right\}; \left\{ c^{(s)} \right\}; \left\{ c^{(T)} \right\}; \left\{ c_{n1} \right\} \right\} \tag{31}$$

On the right-hand side of Eq. (29), the first three terms represent the translational rigid body motion, singular stress term and T-stress term, respectively. For the fourth term, the real parts of the eigenvalues in $-[S_{n1}]$ are all larger than one, which will not lead to the singularity. It can be seen from Eq. (30) that the first term of $\{u(\xi)\}_{,\xi}$ will lead to singularities when $\xi \rightarrow 0$, because the real parts of the eigenvalues in $[S^{(s)}]$ are between -1 and 0.

The calculation of stresses from the displacements field is similar to that in the FEM. At a specified local coordinate s of a line element, the stress fields are expressed as

$$\begin{aligned} \{\sigma(\xi, s)\} &= [\psi_\sigma^{(s)}(s)] \xi^{-[S^{(s)}]-[I]} \{c^{(s)}\} \\ &+ [\psi_\sigma^{(T)}(s)] \{c^{(T)}\} + o(1) \end{aligned} \quad (32)$$

with

$$[\psi_\sigma^{(s)}(s)] = [D] \left(-[B^1(s)] [\psi^{(s)}] [S^{(s)}] + [B^2(s)] [\psi^{(s)}] \right) \quad (33a)$$

$$[\psi_\sigma^{(T)}(s)] = [D] \left([B^1(s)] [\psi^{(T)}] [S^{(s)}] + [B^2(s)] [\psi^{(T)}] \right) \quad (33b)$$

where $[\psi_\sigma^{(s)}(s)]$ and $[\psi_\sigma^{(T)}(s)]$ are the singular stress and T-stress terms, respectively. $[D]$ is the elasticity matrix and $[B^1(s)]$ and $[B^2(s)]$ are relevant matrices. Analogous to $O(\xi^n)$, $o(\xi^n)$ stands for a function that tends to zero more rapidly than ξ^n when $\xi \rightarrow 0$. Because the fourth term in Eq. (29) has no relationship with the singular stress, its contribution to stresses is in the order $o(1)$ and not explicitly given in Eq. (32). As to the translational rigid body motions (the first term in Eq. (29)), it do not induce stresses. The asymptotic solution of the stress around the singular point shows that the singular stresses and T-stress are the same as the static counterparts. After obtaining the integration constants $\{c\}$, the definitions of the stress intensity factors and T-stress for the static problems can be directly applied to the dynamic problems.

3.2 Numerical solution for internal displacement and stress in the time domain

For the dynamic case, the integration constants $\{c\}$ cannot be obtained directly using the nodal displacements on the boundary from Eq. (28), because the high order term $o(\xi^2)$ should be considered unless the size of the subdomains is small enough Song (2004b). Therefore, the displacements and stresses around the crack tip ($\xi \rightarrow 0$) are necessary for calculating the integration constants, especially when the size of the subdomains is larger. In this paper, a numerical procedure based on the improved continued fraction solution is employed to solve this problem in the time domain.

Substituting Eq. (2) into Eq. (26b), the equation of motion in the time domain can be rewritten as a system of first-order differential-algebraic equations for the displacement functions $\{u(\xi)\}$

$$\begin{aligned} \begin{Bmatrix} [E^0] \xi \{u(\xi)\}_{,\xi} \\ 0 \\ 0 \\ \vdots \\ 0 \\ 0 \end{Bmatrix} &= \begin{bmatrix} [K] - [E^1]^T & 0 & 0 & \cdots & 0 & 0 \\ 0 & [S_0^{(1)}] & 0 & \cdots & 0 & 0 \\ 0 & 0 & [S_0^{(2)}] & \cdots & 0 & 0 \\ \vdots & \vdots & \vdots & \ddots & \vdots & \vdots \\ 0 & 0 & 0 & \cdots & [S_0^{(M_{cf}-1)}] & 0 \\ 0 & 0 & 0 & \cdots & 0 & [S_0^{(M_{cf})}] \end{bmatrix} \begin{Bmatrix} \{u(\xi)\} \\ \{u^{(1)}(\xi)\} \\ \{u^{(2)}(\xi)\} \\ \vdots \\ \{u^{(M_{cf}-1)}(\xi)\} \\ \{u^{(M_{cf})}(\xi)\} \end{Bmatrix} \\ + \xi^2 \begin{bmatrix} [M] & -[X^{(1)}] & 0 & \cdots & 0 & 0 \\ -[X^{(1)}]^T & [S_1^{(1)}] & -[X^{(2)}] & \cdots & 0 & 0 \\ 0 & -[X^{(2)}]^T & [S_1^{(2)}] & \cdots & 0 & 0 \\ \vdots & \vdots & \vdots & \ddots & -[X^{(M_{cf}-1)}] & 0 \\ 0 & 0 & 0 & -[X^{(M_{cf}-1)}]^T & [S_1^{(M_{cf}-1)}] & -[X^{(M_{cf})}] \\ 0 & 0 & 0 & 0 & -[X^{(M_{cf})}]^T & [S_1^{(M_{cf})}] \end{bmatrix} \begin{Bmatrix} \{\ddot{u}(\xi)\} \\ \{\ddot{u}^{(1)}(\xi)\} \\ \{\ddot{u}^{(2)}(\xi)\} \\ \vdots \\ \{\ddot{u}^{(M_{cf}-1)}(\xi)\} \\ \{\ddot{u}^{(M_{cf})}(\xi)\} \end{Bmatrix} \end{aligned} \quad (34)$$

It is an initial value problem with the initial value defined at $\xi=1$ by the nodal displacements $\{u(\xi=1)\}$ and auxiliary variables $\{u^{(i)}(\xi=1)\}$, ($i=1, 2, \dots, M_{cf}$).

Combining Eq. (10) and the first submatrix of the decomposition in Eq. (9) yield

$$[E^0]^{-1} \left([K] - [E^1]^T \right) = -[V_{11}] [S_{11}] [V_{11}]^{-1} \quad (35)$$

Then the derivative $\xi \{u(\xi)\}_{,\xi}$ for the improved continued fraction solution can be derived from the first row block of Eq. (34) with Eq. (35) as

$$\begin{aligned} \xi \{u(\xi)\}_{,\xi} &= -[V_{11}] [S_{11}] [V_{11}]^{-1} \{u(\xi)\} \\ &+ \xi^2 [E^0]^{-1} [M] \{\ddot{u}(\xi)\} \\ &- \xi^2 [E^0]^{-1} [X^{(1)}] \{\ddot{u}^{(1)}(\xi)\} \end{aligned} \quad (36)$$

To compute accurately the internal displacements with the initial value equation, the singularity in $\{u(\xi)\}_{,\xi}$ corresponding to the stress singularity (Eq. (30)) should be removed analytically by introducing the following variable

$$\{v(\xi)\} = \xi^{[S_v]} [V_{11}]^{-1} \{u(\xi)\} \quad (37)$$

where the matrix $[S_v]$ partitioned conformably with $[S_{11}]$ in Eq. (11) is defined as

$$[S_v] = \text{diag} \left(0, -[I], [S^{(s)}], 0 \right) \quad (38)$$

where the diagonal block $[S^{(s)}]$ corresponds to the singular stress term and the identity matrix $[I]$ are used for evaluating the T-stress. Substituting Eq. (28) with Eq. (11) into Eq. (37) lead to the asymptotic solution for $\{v(\xi)\}$

$$\begin{aligned} \{v(\xi)\} &= \xi^{[S_v]} \left(\xi^{-[S_{v1}]} \{c\} + O(\xi^2) \right) \\ &= \text{diag} \left(\xi^{-[S_{v1}]} [I], [I], [I], [I] \right) \{c\} + O(\xi) \end{aligned} \quad (39)$$

$\{v(\xi)\}_{,\xi}$ is thus without the stress singularity.

Eliminating $\{u(\xi)\}$ with Eq. (37), Eq. (36) can be rewritten as

$$\begin{aligned} \xi \{v(\xi)\}_{,\xi} &= (-[S_{11}] + [S_v]) \{v(\xi)\} \\ &+ \xi^2 \xi^{[S_v]} [V_{11}]^{-1} [E^0]^{-1} [M] [V_{11}] \xi^{-[S_v]} \{\ddot{v}(\xi)\} \\ &- \xi^2 \xi^{[S_v]} [V_{11}]^{-1} [E^0]^{-1} [X^{(1)}] \{\ddot{v}^{(1)}(\xi)\} \end{aligned} \quad (40)$$

Then Eq. (34) is reformed by replacing the equations in the first row block with Eq. (40) and adding the variable $\{v(\xi)\}$ to the equations in the second row block as

$$[A] \{D(\xi)\} + [B(\xi)] \{\ddot{D}(\xi)\} = [C] \xi \{D(\xi)\}_{,\xi} \quad (41)$$

where $\{D(\xi)\}$ is a column vector formed by concatenating $\{v(\xi)\}$ and auxiliary variables

$$\{u^{(i)}(\xi=1)\}, \quad (i=1, 2, \dots, M_{cf})$$

$$\{D(\xi)\} = \left\{ \{v(\xi)\}; \{u^{(1)}(\xi)\}; \{u^{(2)}(\xi)\}; \dots; \{u^{(M_{cf})}(\xi)\} \right\} \quad (42)$$

The coefficient matrices are defined as

$$[A] = \text{diag} \left(-[S_{11}] + [S_v], [S_0^{(1)}], [S_0^{(2)}], \dots, [S_0^{(M_{cf})}] \right) \quad (43a)$$

$$[B(\xi)] = \begin{bmatrix} \xi^{\xi[S_v]} [V_{11}]^{-1} [E^0]^{-1} [M] [V_{11}] \xi^{-1[S_v]} - \xi^{\xi[S_v]} [V_{11}]^{-1} [E^0]^{-1} [X^{(1)}] & 0 & \dots & 0 \\ -[X^{(1)}] [V_{11}] \xi^{-1[S_v]} & [S_1^{(1)}] & -[X^{(2)}] \dots & 0 \\ 0 & -[X^{(2)}]^T & [S_1^{(2)}] \dots & 0 \\ \vdots & \vdots & \vdots & \ddots \\ 0 & 0 & 0 & \dots [S_1^{(M_{cf})}] \end{bmatrix} \quad (43b)$$

$$[C] = \begin{bmatrix} [I] & 0 \\ 0 & 0 \end{bmatrix} \quad (43c)$$

The initial condition for Eq. (40) is obtained at $\xi=1$ from Eq. (37)

$$\{v(\xi=1)\} = [V_{11}]^{-1} \{u(\xi=1)\} \quad (44)$$

and the solution of Eq. (34) for auxiliary variables on the boundary $\{u^{(i)}(\xi=1)\}$, ($i=1, 2, \dots, M_{cf}$).

Analogous to the matrices $[M_b]$, the block-diagonal terms of coefficient matrices $[B(\xi)]$ may strongly differ in magnitude when the order of continued fraction is increased, which will lead to ill-conditioning and inefficiency during the calculation.

Using the initial condition, the initial value problem of Eq. (41) can be solved numerically at discrete values of radial coordinate ξ_j ($j=1, 2, \dots, n$) ranging from $\xi_1=1$ on the boundary to ξ_n at the scaling center. For numerical stability, a very small value, i.e., 10^{-6} , instead of being equal to zero exactly, is chosen for ξ_n . The matrix power functions $\xi^{-[S_v]}$ in coefficient matrix $[B(\xi)]$ are calculated as matrix exponential $\exp(-[S_v] \ln \xi)$ using the “scaling and squaring” algorithm (Song 2004a), which is capable of representing power-logarithmic singularities. A Newmark-like scheme with a numerical factor $\gamma \xi$, which is proposed in Song and Vrcelj (2008), is applied to a typical interval $\Delta \xi = \xi_{j+1} - \xi_j$

$$\{D(\xi_{j+1})\} = \{D(\xi_j)\} + (1 - \gamma \xi) \Delta \xi \{D(\xi_j)\}_{,\xi} + \gamma \xi \Delta \xi \{D(\xi_{j+1})\}_{,\xi} \quad (45)$$

The size of the interval $\Delta \xi$ is chosen based on the shortest wavelength that a mesh can represent. A sensitivity analyses is performed by choosing $\Delta \xi$ to divide the shortest wavelength into 10-20 internals. The result is not appreciably affected by the different interval parameters. In

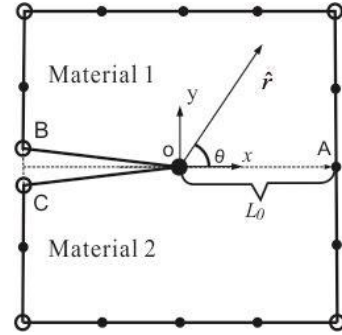


Fig. 2 A cracked subdomain modelled by the SBFEM

the numerical examples of this paper, $\Delta \xi$ is chosen by dividing the shortest wavelength into 13 internals. Substituting Eq. (45) into Eq. (41), the equation for $\{D(\xi_{j+1})\}$ is expressed as

$$\left(-[A] + \frac{\xi_{j+1}}{\gamma \xi \Delta \xi} [C] \right) \{D(\xi_{j+1})\} - [B(\xi_{j+1})] \{D(\xi_{j+1})\}_{,\xi} = \frac{\xi_{j+1}}{\gamma \xi \Delta \xi} [C] \left(\{D(\xi_j)\} + (1 - \gamma \xi) \Delta \xi \{D(\xi_{j+1})\}_{,\xi} \right) \quad (46)$$

After applying the Newmark scheme in a time interval $\Delta t = t_{k+1} - t_k$

$$\{\dot{D}(\xi_j)\}_{k+1} = \{\dot{D}(\xi_j)\}_k + (1 - \gamma) \Delta t \{\ddot{D}(\xi_j)\}_k + \gamma \Delta t \{\ddot{D}(\xi_j)\}_{k+1} \quad (47a)$$

$$\{D(\xi_j)\}_{k+1} = \{D(\xi_j)\}_k + \Delta t \{\dot{D}(\xi_j)\}_k + \left(\frac{1}{2} - \beta \right) \Delta t^2 \{\ddot{D}(\xi_j)\}_k + \beta \Delta t^2 \{\ddot{D}(\xi_j)\}_{k+1} \quad (47b)$$

All discrete internal displacement values of the radial coordinate ξ_j ($j=2, 3, \dots, n$) at a specified time can be obtained by looping the following equation

$$\left(-[A] + \frac{\xi_{j+1}}{\gamma \xi \Delta \xi} [C] - \frac{1}{\beta \Delta t^2} [B(\xi_{j+1})] \right) \{D(\xi_{j+1})\}_{k+1} = \frac{\xi_{j+1}}{\gamma \xi \Delta \xi} [C] \left(\{D(\xi_j)\}_{k+1} + (1 - \gamma \xi) \Delta \xi \{D(\xi_{j+1})\}_{,\xi} \right) - \frac{1}{\beta \Delta t^2} [B(\xi_{j+1})] \left(\{D(\xi_{j+1})\}_k + \Delta t \{\dot{D}(\xi_{j+1})\}_k + \left(\frac{1}{2} - \beta \right) \Delta t^2 \{\ddot{D}(\xi_{j+1})\}_k \right) \quad (48)$$

and the internal stresses follow from Eq. (32).

For later use, defining the coefficient matrix $[G_{j+1}]$ as

$$[G_{j+1}] = \left(-[A] + \frac{\xi_{j+1}}{\gamma \xi \Delta \xi} [C] - \frac{1}{\beta \Delta t^2} [B(\xi_{j+1})] \right) \quad (49)$$

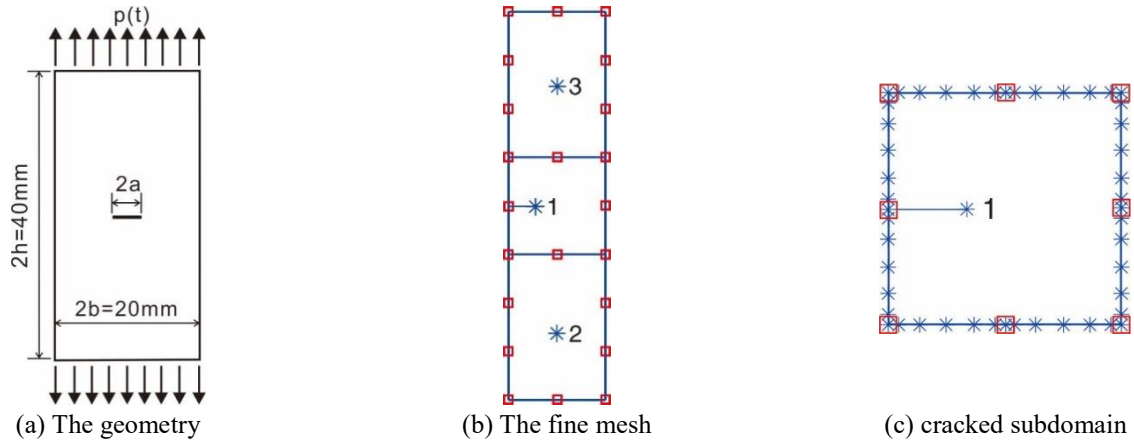


Fig. 3 A rectangular plate with a central crack

Now, the integration constants $\{c\}$ can be obtained directly from the solution at the scaling center $\{D(\xi=0)\}$ by using Eq. (39)

$$\{v(\xi=0)\} = \{0; \{c^{(T)}\}; \{c^{(s)}\}; \{c^{(r)}\}\} \quad (50)$$

The stress intensity factors and T-stress for the dynamic problems is then calculated according to their definitions with the integration constants in Eq. (50).

4. Evaluation the dynamic stress intensity factors and T-stress

Fig. 2 shows a cracked subdomain modeled by the SBFEM, in which the origins of the Cartesian and polar coordinate systems are located at the crack tip. Without losing generality, the x-axis is along the line of the crack. For the crack in a homogeneous plate and interfacial crack in an isotropic bimaterial plate, the definitions of stress intensity factors are well accepted and appear repeatedly in the literature. They can be defined using the uniform form as

$$\begin{Bmatrix} \sigma_{\theta\theta}^{(s)}(\hat{r}, 0) \\ \tau_{r\theta}^{(s)}(\hat{r}, 0) \end{Bmatrix} = \frac{1}{\sqrt{2\pi\hat{r}}} \begin{bmatrix} c(\hat{r}) & -s(\hat{r}) \\ s(\hat{r}) & c(\hat{r}) \end{bmatrix} \begin{Bmatrix} K_{\perp} \\ K_{\parallel} \end{Bmatrix} \quad (51)$$

with

$$c(\hat{r}) = \cos(\varepsilon \ln(\hat{r}/L)); \quad s(\hat{r}) = \sin(\varepsilon \ln(\hat{r}/L)) \quad (52)$$

where L is a characteristic length and ε is the oscillatory index which depends on the material properties. When the oscillatory index is equal to zero, Eq. (51) is used for calculating the SIFs of cracks in homogeneous plates.

After introducing the polar coordinates \hat{r} and θ , the local coordinate ξ is expressed as

$$\xi = \hat{r} / r(\theta) = (L / r(\theta)) \times (\hat{r} / L) \quad (53)$$

Where $r(\theta)$ is the distance from the scaling center to the boundary along the radial line at angle θ (such as the L_0 in Fig. 2) The matrix power function of ξ in Eqs. (32) and (33)

is rewritten into the polar coordinate as

$$\xi^{-[s^{(s)}]-[I]} = (L / r(\theta))^{-[s^{(s)}]-[I]} (\hat{r} / L)^{-[s^{(s)}]-[I]} \quad (54)$$

The singular stress term (Eq. (33)) is transformed from the local coordinates to the polar coordinates using the standard procedure with Eq. (54)

$$\begin{aligned} \{\sigma^{(s)}(\hat{r}, \theta)\} &= [\psi_{\sigma L}^{(s)}(\theta)] \left((\hat{r} / L)^{-[s^{(s)}]-[I]} \right) \{c^{(s)}\}; \\ [\psi_{\sigma L}^{(s)}(\theta)] &= [\psi_{\sigma}^{(s)}(s)] (L / r(\theta))^{-[s^{(s)}]-[I]} \end{aligned} \quad (55)$$

According to the uniform form of stress intensity factors in Eq. (51), the generalized stress intensity factors are expressed in Song *et al.* (2010a) as

$$\{K(\theta)\} = \sqrt{2\pi L} [\psi_{\sigma L}^{(s)}(\theta)] \{c^{(s)}\} \quad (56)$$

The stress intensity factors can be easily evaluated by using Eq. (56) at any given angle, which is useful and convenient in determining the direction of crack propagation. This definition is valid to cracks in homogeneous plates and interfacial cracks in isotropic bimaterials with the same form. A point in front of the crack tip on the boundary (i.e., the point A in Fig. 2) is normally used to evaluate the SIFs with Eq. (56), in which the θ is equal to zero.

The T-stress term in Eq. (33b) is independent of the radial coordinate ξ . At the point A, it is written as

$$\{\sigma^{(T)}(\xi, \theta=0)\} = [\psi_{\sigma}^{(T)}(s(\theta=0))] \{c^{(T)}\} \quad (57)$$

The T-stress is simply the xx component based on its definition

$$T = \sigma_{xx}^{(T)} \quad (58)$$

Note that the order and type of the singularity are not directly used with the generalized stress intensity factors and no asymptotic solution of the stress field is required during the calculation.

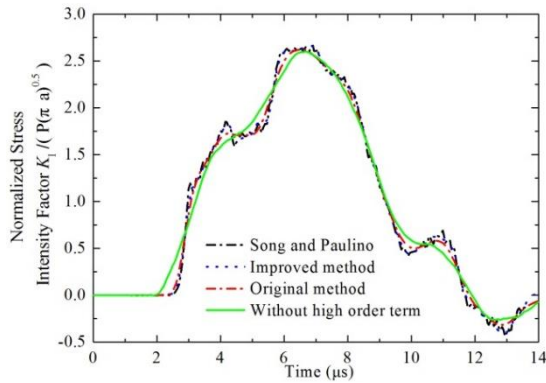


Fig. 4 Dynamic stress intensity factor

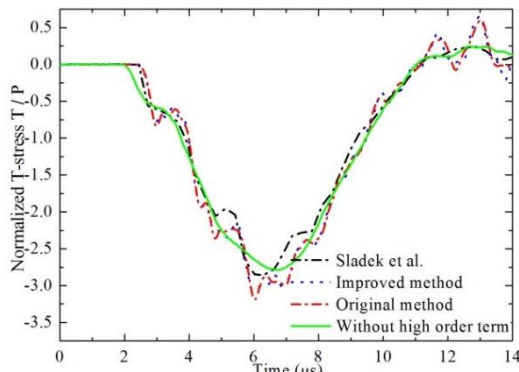


Fig. 5 Dynamic T-stress

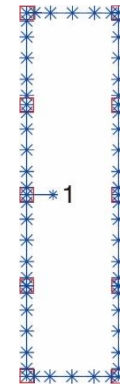


Fig. 6 The coarse mesh

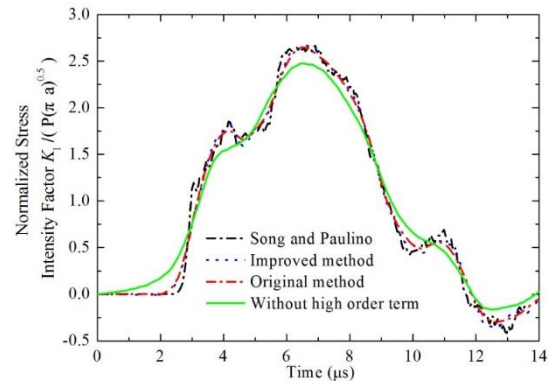


Fig. 7 Dynamic stress intensity factor of coarse mesh

5. Numerical examples

Three numerical examples are presented in the following to demonstrate the efficiency and robustness of the technique developed in this paper. In the first example, the dynamic stress intensity factors and T-stress of a central crack in a rectangular plate are analyzed. The improved robustness of the proposed continued fraction solution including a scaling factor compared to the original approach is demonstrated. In the following examples, a rectangular plate with an inclined central crack, and a bi-material plate with a crack at the material interface are addressed respectively. It is shown that the DSIFs and T-stress extracted by the proposed method agree well with the published results and the solution procedure is more efficient. In all calculations, the parameters $\gamma_\xi=2/3$, $\gamma=1/2$ and $\beta=1/4$ are chosen in the numerical integration. The computational efficiency is evaluated by comparing the CPU time record on a laptop computer with Intel Core i5-4200M CPU @ 2.50 GHz and 4 GB RAM.

5.1 Rectangular plate with a central crack

A rectangular plate with a central crack is subjected to uniform tractions on its top and bottom edges with a step Heaviside function $p(t)=PH(t)$, where P is the magnitude of the uniform tractions. The geometry and boundary conditions are shown in Fig. 3(a). The crack length is $2a=4.8$ mm. The elastic material properties are: shear modulus $G=76.923$ Gpa, Poisson's ratio $\nu=0.3$ and mass density $\rho=5 \times 10^{-6}$ kg/mm³. Plane strain condition is

considered.

Two meshes are employed in the scaled boundary finite element analysis. To enable the use of the same mesh in comparing with the original results and modeling the bi-material plate in Section 5.3, half of the plate is discretized with three subdomains as the fine mesh. The cracked subdomain has its scaling center at the crack tip and the others at their geometrical centers. The seven-node line elements with Gauss-Lobatto-Legendre shape functions are used to discretize the boundary. The two nodes at the ends of each line element are shown in Fig. 3(b). Fig. 3(c) shows the detail of the boundary mesh of the cracked subdomain with the nodes indicated by the markers '*'. All DSIFs reported below are normalized by a factor $P\sqrt{\pi a}$ where a is the half crack length.

In general, a sufficiently boundary nodes and a sufficiently high order of continued fraction expansion are required to accurately represent higher order modes. According to the parametric study in Song (2009), six nodes and 3-4 terms of continued fraction for one wavelength lead to highly accurate results. For the fine mesh, the length of the line element is equal to 5 mm, and then the shortest wavelength that the mesh can model is about 5 mm. The largest distance between the scaling center and a point on the boundary is about 9 mm, which is about 1.8 wavelengths. Based on the largest distance, the order of the continued fraction is chosen as $M_{cf}=5$. Considering the dilatational wave velocity $c_p=7.338$ mm/ μ s, the period of the shortest wave is about 0.68 μ s. A time step $\Delta t=0.05$ μ s is selected, which corresponds to about 13 steps in one period

Table 1 Condition numbers with respect to the coefficient matrices $[S_0^{(i)}]$ and $[G_j]$

i/j	Original method				Improved method	
	$[S_0^{(i)}]$	$[G_j]: M_{cf}=6$	$[G_j]: M_{cf}=8$	$[G_j]: M_{cf}=10$	$[S_0^{(i)}]$	$[G_j]$
1	1.04E06	1.76E09	2.64E12	1.97E14	190.27	3.46E05
2	1.83E05	1.85E09	2.31E12	1.68E14	82.73	3.03E05
3	6.69E05	1.97E09	1.97E12	1.46E14	84.73	2.61E05
4	3.71E06	2.13E09	1.65E12	1.95E14	39.46	2.19E05
5	2.86E07	2.34E09	1.32E12	9.72E13	44.46	1.79E05
6	4.69E09	2.62E09	1.01E12	8.79E13	27.67	1.39E05
7	6.44E09	2.98E09	7.02E11	4.61E13	36.91	1.01E05
8	6.03E10	3.43E09	4.16E11	3.10E13	34.90	6.57E04
9	7.42E10	3.95E09	1.76E11	2.85E13	35.48	3.46E04
10	2.73E11	4.45E09	7.72E10	1.05E14	31.70	1.08E04

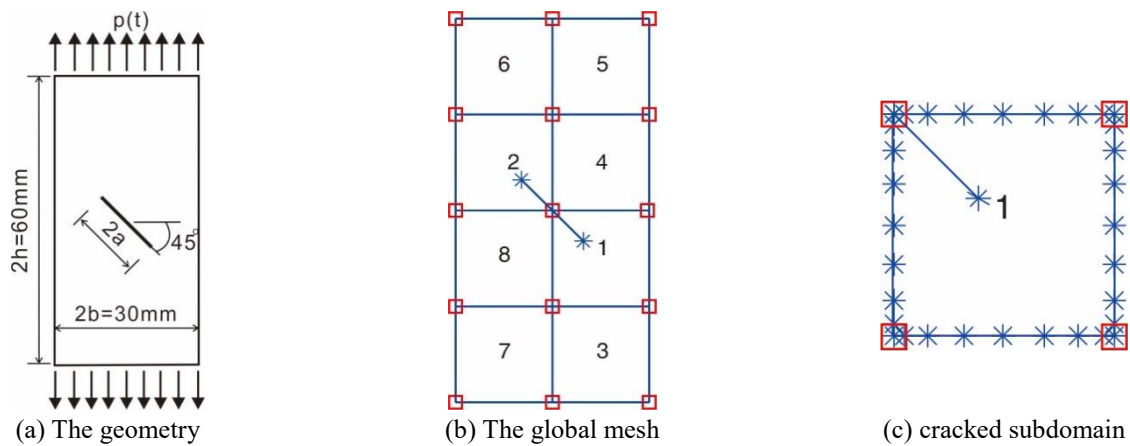


Fig. 8 A rectangular plate with an inclined central crack

of the shortest wave. In computing the internal displacement, the numerical integration over ζ is performed with $\Delta\zeta=0.05$ so that the shortest wavelength is divided into around 13 internals.

Fig. 4 shows the dynamic stress intensity factor obtained by using the improved continued fraction method with the fine mesh as a dotted line. Very good agreement with the original method (Song and Vrcelj 2008) result and the finite element result (Song and Paulino 2006) is achieved. The small amplitude oscillations at very high frequency (the period is about $0.3 \mu\text{s}$, which is shorter than the shortest wavelength the mesh can represent) in the FE solution do not appear in both the present and original results. The computer time for the present technique is 44.9 s and it is mostly spent on computing the internal displacements and extracting the dynamic stress intensity factors (41.8 s). The time spent computing the original method solution is about 86.6 s, out of which, 82.2 s is spent on calculating the fracture parameters. Obviously, the improved continued fraction approach is competitive in terms of efficiency in a dynamic analysis, especially for the fracture problems. In order to consider the effect of the high order term on the dynamic problems, the DSIFs calculated with the integration constants $\{c\}$, which are obtained by using Eq.

(28) with the boundary displacements directly, is also shown in Fig. 4 by the solid line. It can be seen that the difference with the FE results is larger and thus calculating the integration constants with the internal displacements can lead to more accurately stress intensity factors results. The dynamic T-stress results for the present and the original approaches are shown in Fig. 5, together with the boundary element results in Sladek *et al.* (1999). The amount of difference in these dynamic T-stress results is similar to that in the dynamic stress intensity factor.

To verify the accuracy and robustness of the present method for the dynamic problems, an analysis is performed using both the original approach and the proposed method with the coarse mesh in Fig. 6. As shown in Fig. 6, the length of the line element is equal to 10 mm and the largest distance between the scaling center and a point on the boundary is about twice as long as the element length. Based on the shortest wavelength that the coarse mesh can represent, the size of integration interval $\Delta\zeta=0.09$ is chosen and the necessary order of continued fraction expansion M_{cf} is 6-10. A parameter study has been performed using these different orders. It was found that both approaches yield identical solutions for the dynamic stress intensity factors, if the order of continued fraction expansion was chosen as

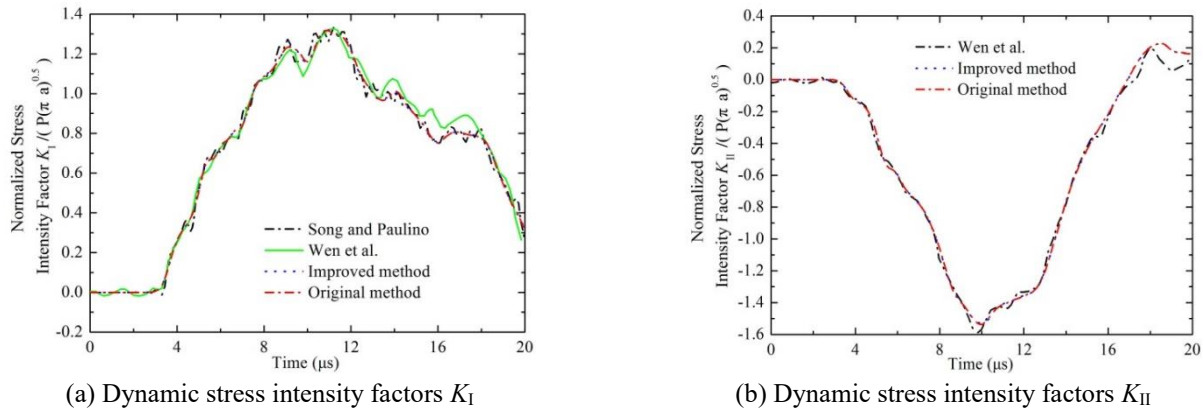


Fig. 9 Dynamic stress intensity factor of rectangular plate with an inclined central crack.

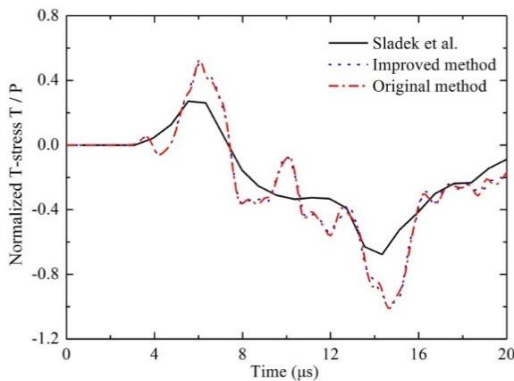


Fig. 10 Dynamic T-stress of rectangular plate with an inclined central crack

$M_{cf}=6,7$. For other higher orders, however, the singular matrices were generated during the calculation procedure using the original approach, which even broke down the programs.

To further illustrate this, the condition numbers with respect to the coefficient matrices $[S_0^{(i)}]$ and $[G_j]$ have been computed for a number of orders and listed in Table 1. Due to the condition numbers computed using proposed method are almost the same with each other regardless of the order of continued fraction expansion, only one series of the proposed method results for $M_{cf}=10$ is shown in Table 1. According to the reference (Chen *et al.* 2014), a matrix is ill-conditioned if its condition number is too large, that is, if it approaches the machine's floating point precision (i.e., 10^{12} for double precision). Table 1 shows that the condition numbers of $[S_0^{(i)}]$ for the proposed approach, which lead to better conditioned and more stable coefficient matrices, are generally much smaller than the $[G_j]$ values obtained using the original approach. For this given problem, the original approach leads to ill-conditioned coefficient matrices and thus the original method breaks down for dynamic fracture analysis, when the continued fraction approximation of order is higher than 7.

When using the coarse mesh and $M_{cf}=6$, the dynamic stress intensity factors obtained by the improved and original method are shown in Fig. 7. Again, good agreement with the reference results in Song and Paulino (2006) is

observed. The CPU time for the improved approach is 63.2 s, which is about half of it for the original approach (117.0 s). This indicates that well-conditioned matrices yielded by the proposed method can lead to a more efficient and robust solution procedure for calculating the dynamic stress intensity factors. It should be noted that the DSIFs calculated without considering the high order term (shown in Fig. 7 as the solid line) have a much bigger difference compared with other three results. It is mainly because the effect of the inertia force becomes more important in a larger size of the cracked subdomain. Therefore, extracting the internal displacements to calculate the integration constants $\{c\}$ are more necessary for obtaining the accurate dynamic results when the size of elements is larger.

5.2 Rectangular plate with an inclined central crack

A rectangular plate with an inclined central crack is shown in Fig. 8(a). The width and height of the plate are $2b=30$ mm and $2h=60$ mm, respectively. The length of the crack is $2a=10\sqrt{2}$ mm. The material properties are the same as those in Section 5.1. Plane strain condition is assumed in this example. The plate is loaded at time $t=0$ by a uniform traction with Heaviside function time dependence $p(t)=PH(t)$.

Fig. 8(b) shows the discretization of this rectangular plate with 8 subdomains. The boundary of each edge is modeled with one nine-node line element. The detail of the cracked subdomain 1 with the nodes indicated by '*' is illustrated in Fig. 8(c). Note that the part of crack faces in this subdomain, whose scaling center is at the crack tip, is not discretized. In the dynamic analysis, a time step $\Delta t=0.1$ μ s is selected. The order of the continued fraction is chosen as $M_{cf}=4$ for all of the subdomains. The numerical integration $\Delta\xi=0.05$ is selected for extracting the internal displacements.

The dynamic stress intensity factors K_I and K_{II} obtained by using the proposed approach and original approach are shown in Fig. 9(a) and (b), respectively. The finite element result (Song and Paulino (2006) (for K_I only) and the boundary element result (Wen *et al.* 1997) are digitized and shown as reference solutions. Very good agreement is observed. The CPU time is 19.8 s for the present technique (where about 16.2 s is spent on calculating the internal

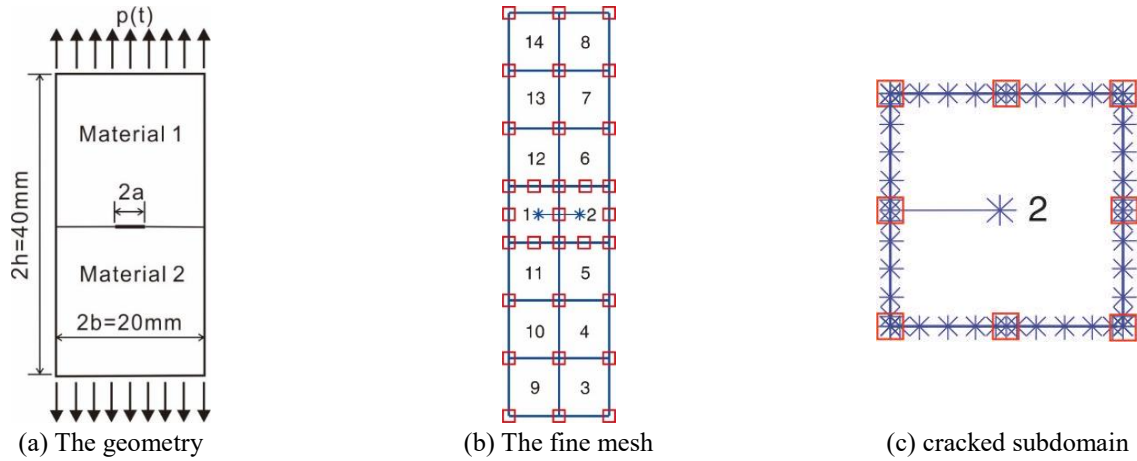


Fig. 11 A rectangular bi-material plate with a central crack

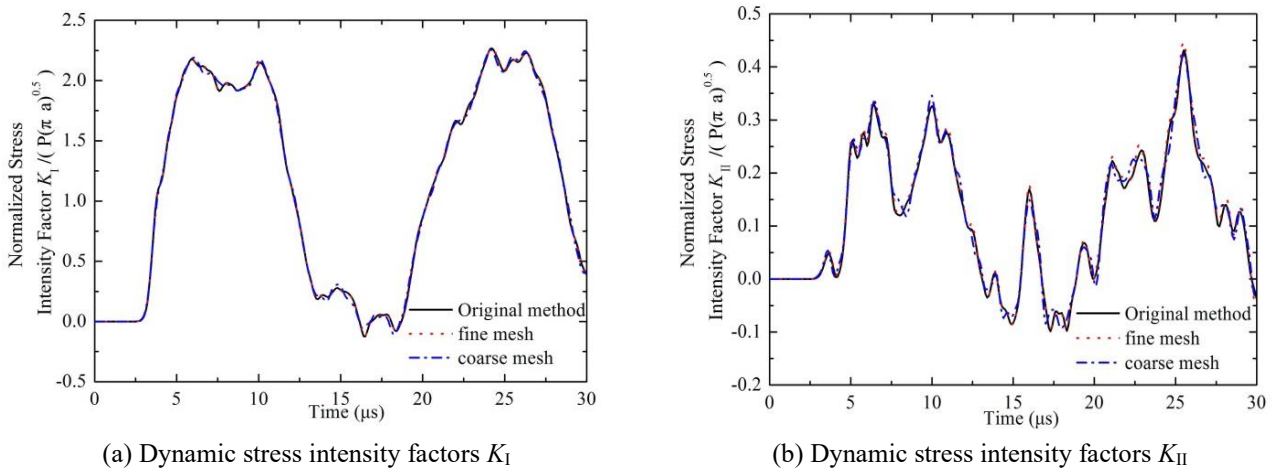


Fig. 12 Dynamic stress intensity factors of rectangular bi-material plate

Table 2 Condition numbers with respect to the coefficient matrices $[S_0^{(i)}]$ and $[G_j]$

i/j	Original method		Improved method	
	$[S_0^{(i)}]$	$[G_j]$	$[S_0^{(i)}]$	$[G_j]$
1	5.40E05	2.45E06	38.32	509.67
2	8.03E04	2.47E06	23.89	464.97
3	3.40E05	2.49E06	18.60	381.63
4	1.36E11	2.52E06	17.73	342.87

displacements and the DSIFs) and 30.5 s for the original method (where about 26.5 s is used to calculating the fracture parameters). Compared with the first example in Section 5.1, the time spent on the procedure is significant reduced along with the reduction of the number of DOFs and the order of continued fraction expansion for the cracked subdomain. The dynamic T-stresses calculated by the two approaches are agreed well with each other as shown in Fig. 10. The result of Sladek *et al.* (1999) is digitized and plotted as the solid line. Considerable difference between the present result and the reference solution exists. Additional analyses with increasing node density are performed by using the improved method. No

appreciable difference with the present result in Fig. 10 is obtained.

As is shown in Table 2, the condition numbers of $[S_0^{(i)}]$ for the improved approach, which lead to better conditioned and more stable coefficient matrices $[G_j]$, are generally much smaller than the values obtained using the original approach.

5.3 Rectangular bi-material plate with a central crack

The final example solved here is a rectangular bimaterial plate with a central crack subjected to uniform tractions on its upper and lower surfaces. The geometry of the plate and the length of the crack are the same as those of the rectangular plate in Section 5.1 and shown in Fig. 11(a). The upper part of the plate is quartz (Material 1) and the lower part is copper (Material 2). The elastic material properties for these two materials are: shear modulus $G_1=47.9$ Gpa, Poisson's ratio $\nu_1=0.058$ and mass density $\rho_1=5 \times 10^{-6}$ kg/mm³; shear modulus $G_2=48.1$ Gpa, Poisson's ratio $\nu_2=0.2976$ and mass density $\rho_2=8.96 \times 10^{-6}$ kg/mm³. In this paper, the response to the step loading $p(t)=PH(t)$ is considered. The coarse mesh (Fig. 3(b)) and the fine mesh with 14 subdomains (Fig. 11(b)) is employed to model this dynamic problem.

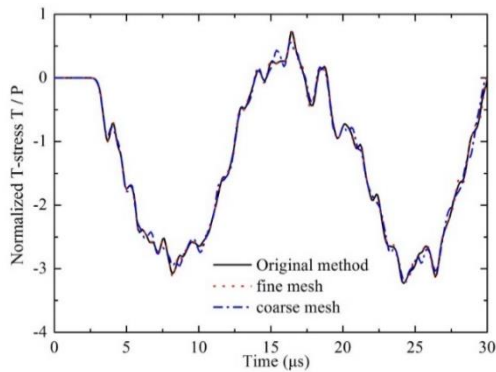


Fig. 13 Dynamic T-stress of rectangular bi-material plate with a central crack

Table 3 Condition numbers with respect to the coefficient matrices $[S_0^{(i)}]$ and $[G_j]$

i/j	Original method		Improved method	
	$[S_0^{(i)}]$	$[G_j]$	$[S_0^{(i)}]$	$[G_j]$
1	1.42E06	1.01E07	43.76	955.96
2	5.22E04	1.03E07	25.12	864.11
3	7.81E05	1.05E07	19.31	776.57
4	2.64E05	1.07E07	15.12	693.37
5	1.81E06	1.10E06	12.07	614.54

The time step is chosen as $\Delta t=0.1 \mu s$, and the transient response up to $30 \mu s$ is considered. The order of continued fraction is selected as $M_{cf}=5$ for all the subdomains. The present results obtained with the coarse mesh and fine meshes are in good agreement with the original result with fine mesh as shown in Fig. 12. Only slight difference of high frequency is observed between results calculated with the two meshes. According to Fig. 13, the dynamic T-stress extracted from the cracked subdomain is similar to the reference results as the DSIFs. Compared the two methods' results with the fine mesh, the total times for calculating the dynamic results with the fine mesh are 59.9 s and 109.0 s, respectively. This example demonstrates that the present technique is also more efficient on computing time histories of dynamic stress intensity factors and T-stress at bimaterial interface cracks than the original method.

As is shown again in Table 3, the condition numbers of $[S_0^{(i)}]$ and $[G_j]$ for the improved are generally much smaller than the values obtained using the original approach, which shows that improved approach is more stable.

6. Conclusions

In this paper, an improved numerical procedure of the scaled boundary finite element method is proposed to calculate the dynamic stress intensity factors and T-stress for two-dimensional crack problems. It is based on an improved continued-fraction expansion of the dynamic stiffness matrix of the bounded domains. After removing

the stress singularity analytically, the corresponding ordinary differential equations for internal displacements are derived and solved by numerical integration. The dynamic stress intensity factors and T-stress are evaluated directly from displacement or stress fields according to their definitions. No mesh refinement is needed close to the singular point. The numerical results demonstrate that the proposed method is more robust and efficient than the original one in the time domain for the cracks in homogeneous and bimaterial plates. The condition numbers of coefficient matrix of the improved method are much smaller than that of the original method, which shows that the improved algorithm can obtain well-conditioned coefficient matrices, and the efficiency of the solution process and its stability can be significantly improved. It is anticipated that when combined with the simple remeshing procedure in the SBFEM as developed by Dai *et al.* (2014), this present approach will yield a very competitive technique for modeling dynamic crack propagation problems with very simple meshes.

Acknowledgments

The authors gratefully acknowledge support for this research from the National Natural Science Foundation of China (Grant No. 11372098, 51579084 and 11132003) and the Fundamental Research Funds for the Central Universities (Grant No. 2017B662X14).

References

- Barsoum, R.S. (1977), "Triangular quarter point elements elastic and perfectly plastic crack tip elements", *Int. J. Numer. Meth. Eng.*, **11**(1), 85-98.
- Belytschko, T., Chen, H., Xu, J. and Zi, G. (2003) "Dynamic crack propagation based on loss of hyperbolicity and a new discontinuous enrichment", *Int. J. Numer. Meth. Eng.*, **58**(12), 1873-1905.
- Chen, D. and Dai, S. (2017), "Dynamic fracture analysis of the soil-structure interaction system using the scaled boundary finite element method", *Eng. Analy. Boundar. Elem.*, **77**, 26-35.
- Chen, D., Birk, C., Song, C. and Du, C. (2014), "A high-order approach for modelling transient wave propagation problems using the scaled boundary finite element method", *Int. J. Numer. Meth. Eng.*, **97**(13), 937-959.
- Chen, Y.M. (1975), "Numerical computation of dynamic stress intensity factors by a Lagrangian finite-difference method", *Eng. Fract. Mech.*, **7**(4), 653-660.
- Chidgzev, S.R. and Deeks, A.J. (2005), "Determination of coefficients of crack tip asymptotic fields using the scaled boundary finite element method", *Eng. Fract. Mech.*, **72**(13), 2019-2036.
- Chidgzev, S.R., Trevelyan, J. and Deeks, A.J. (2008), "Coupling of the boundary element method and the scaled boundary finite element method for computations in fracture mechanics", *Comput. Struct.*, **86**(11-12), 1198-1203.
- Chiong, I., Ooi, E.T., Song, C. and Tin-Loi, F. (2014), "Scaled boundary polygons with application to fracture analysis of functionally graded materials", *Int. J. Numer. Meth. Eng.*, **98**(8), 562-589.
- Dai, S., Augarde, C., Du, C. and Chen, D. (2014), "A fully automatic polygon scaled boundary finite element method for

- modelling crack propagation”, *Eng. Fract. Mech.*, **133**, 163-178.
- Fedelinski, P. (2010), “Computer modelling of dynamic fracture experiments”, *Key Eng. Mater.*, **454**, 113-125.
- Jiang, S., Du, C., Gu, C. and Chen, X. (2014), “XFEM analysis of the effects of voids, inclusions and other cracks on the dynamic stress intensity factor of a major crack”, *Atig. Fract. Eng. Mater. Struct.*, **37**(8), 866-882.
- Jiang, S., Du, C. and Gu, C. (2014), “An investigation into the effects of voids, inclusions and minor cracks on major crack propagation by using XFEM”, *Struct. Eng. Mech.*, **49**(5), 597-618.
- Jamal-Omidi, M., Falah, M. and Taherifar, D. (2014), “3-D fracture analysis of cracked aluminum plates repaired with single and double composite patches using XFEM”, *Struct. Eng. Mech.*, **50**(4), 525-539.
- Legrain, G., Cartraud, P., Perreard, I. and Moës, N. (2011), “An X-FEM and level set computational approach for image-based modelling: Application to homogenization”, *Int. J. Numer. Meth. Eng.*, **86**(7), 915-934.
- Li, C., Ooi, E.T., Song, C. and Natarajan, S. (2015), “SBFEM for fracture analysis of piezoelectric composites under thermal load”, *Int. J. Sol. Struct.*, **52**, 114-129.
- Li, C. and Tong, L. (2015), “A mixed SBFEM for stress singularities in nearly incompressible multi-materials”, *Comput. Struct.*, **157**, 19-30.
- Murti, V. and Valliappan, S. (1986), “The use of quarter point element in dynamic crack analysis”, *Eng. Fract. Mech.*, **23**(3), 585-614.
- Natarajan, S. and Song, C. (2013), “Representation of singular fields without asymptotic enrichment in the extended finite element method”, *Int. J. Numer. Meth. Eng.*, **96**(13), 813-841.
- Natarajan, S., Song, C. and Belouettar, S. (2014), “Numerical evaluation of stress intensity factors and T-stress for interfacial cracks and cracks terminating at the interface without asymptotic enrichment”, *Comput. Meth. Appl. Mech. Eng.*, **279**, 86-112.
- Ooi, E.T., Natarajan, S., Song, C. and Ooi, E.H. (2017), “Crack propagation modelling in concrete using the scaled boundary finite element method with hybrid polygon-quadtrees meshes”, *Int. J. Fract. Jan.*, **203**(1-2), 135-157.
- Ooi, E.T., Song, C. and Natarajan, S. (2016), “Construction of high-order complete scaled boundary shape functions over arbitrary polygons with bubble functions”, *Int. J. Numer. Meth. Eng.*, **108**(9), 1086-1120.
- Ooi, E.T., Man, H., Natarajan, S. and Song, C. (2015), “Adaptation of quadtree meshes in the scaled boundary finite element method for crack propagation modelling”, *Eng. Fract. Mech.*, **144**, 101-117.
- Ooi, E.T., Shi, M., Song, C., Tin-Loi, F. and Yang, Z.J. (2013), “Dynamic crack propagation simulation with scaled boundary polygon elements and automatic remeshing technique”, *Eng. Fract. Mech.*, **106**, 1-21.
- Ooi, E.T. and Yang, Z.J. (2011), “Modelling dynamic crack propagation using the scaled boundary finite element method”, *Int. J. Numer. Meth. Eng.*, **88**(4), 329-349.
- Portela, A., Aliabadi, M.H. and Rooke, D.P. (1993), “Dual boundary element incremental analysis of crack propagation”, *Comput. Struct.*, **46**(2), 237-247.
- Réthoré, J., Gravouil, A. and Combescure, A. (2004), “A stable numerical scheme for the finite element simulation of dynamic crack propagation with remeshing”, *Comput. Meth. Appl. Mech. Eng.*, **193**(42), 4493-4510.
- Rabczuk, T. and Belytschko, T. (2006), “Application of particle methods to static fracture of reinforced concrete structures”, *Int. J. Fract.*, **137**(1-4), 19-49.
- Rabczuk, T., Gracie, R., Song, J. and Belytschko, T. (2009), “Immersed particle method for fluid-structure interaction”, *Int. J. Numer. Meth. Eng.*, **81**(1), 48-71.
- Rabczuk, T., Zi, G., Bordas, S. and Nguyen-Xuan, H. (2008), “A geometrically non-linear three-dimensional cohesive crack method for reinforced concrete structures”, *Eng. Fract. Mech.*, **75**(16), 4740-4758.
- Rao, B.N. and Rahman, S. (2004), “An enriched meshless method for non-linear fracture mechanics”, *Int. J. Numer. Meth. Eng.*, **59**(2), 197-223.
- Rice, J.R. (1967), “A path independent integral and the approximate analysis of strain concentration by notches and cracks”, *J. Appl. Mech.*, **35**(2), 379-386.
- Saputra, A., Talebi, H., Tran, D., Birk, C. and Song, C. (2017), “Automatic image-based stress analysis by the scaled boundary finite element method”, *Int. J. Numer. Meth. Eng.*, **109**(5), 697-738.
- Simpson, R. and Trevelyan, J. (2011), “A partition of unity enriched dual boundary element method for accurate computations in fracture mechanics”, *Comput. Meth. Appl. Mech. Eng.*, **200**(1-4), 1-10.
- Sladek, J., Sladek, V. and Fedelinski, P. (1999), “Computation of the second fracture parameter in elastodynamics by the boundary element method”, *Adv. Eng. Softw.*, **30**(9-11), 725-734.
- Song, C. (2004a), “A matrix function solution for the scaled boundary finite-element equation in statics”, *Comput. Meth. Appl. Mech. Eng.*, **193**(23-26), 2325-2356.
- Song, C. (2004b), “A super-element for crack analysis in the time domain”, *Int. J. Numer. Meth. Eng.*, **61**(8), 1332-1357.
- Song, C. (2009), “The scaled boundary finite element method in structural dynamics”, *Int. J. Numer. Meth. Eng.*, **77**(8), 1139-1171.
- Song, C., Tin-Loi, F. and Gao, W. (2010a), “A definition and evaluation procedure of generalized stress intensity factors at cracks and multi-material wedges”, *Eng. Fract. Mech.*, **77**(12), 2316-2336.
- Song, C., Tin-Loi, F. and Gao, W. (2010b), “Transient dynamic analysis of interface cracks in anisotropic bimaterials by the scaled boundary finite-element method”, *Int. J. Sol. Struct.*, **47**(7-8), 978-989.
- Song, C. and Vrcelj, Z. (2008), “Evaluation of dynamic stress intensity factors and T-stress using the scaled boundary finite-element method”, *Eng. Fract. Mech.*, **75**(8), 1960-1980.
- Song, C. and Wolf, J.P. (1997), “The scaled boundary finite-element method-alias consistent infinitesimal finite-element cell method-for elastodynamics”, *Comput. Meth. Appl. Mech. Eng.*, **147**(3-4), 329-355.
- Song, C.M. and Wolf, J.P. (2000), “The scaled boundary finite-element method-a primer: Solution procedures”, *Comput. Struct.*, **78**(1-3), 211-225.
- Song, C.M. and Wolf, J.P. (2002), “Semi-analytical representation of stress singularities as occurring in cracks in anisotropic multi-materials with the scaled boundary finite-element method”, *Comput. Struct.*, **80**(2), 183-197.
- Song, S.H. and Paulino, G.H. (2006), “Dynamic stress intensity factors for homogeneous and smoothly heterogeneous materials using the interaction integral method”, *Int. J. Sol. Struct.*, **43**(16), 4830-4866.
- Wen, P.H., Aliabadi, M.H. and Rooke, D.P. (1997), “A contour integral method for dynamic stress intensity factors”, *Heoret. Appl. Fract. Mech.*, **27**(1), 29-41.
- Wolf, J.P. and Song, C.M. (2000), “The scaled boundary finite-element method-a primer: Derivations”, *Comput. Struct.*, **78**(1-3), 191-210.
- Xiao, Q.Z., Karihaloo, B.L. and Liu, X.Y. (2004), “Direct determination of SIF and higher order terms of mixed mode cracks by a hybrid crack element”, *Int. J. Fract.*, **125**(3-4), 207-225.
- Yang, Z.J. and Deeks, A.J. (2008), “Calculation of transient

- dynamic stress intensity factors at bimaterial interface cracks using a SBFEM-based frequency-domain approach”, *Sci. Chin. Ser. G: Phys. Mech. Astronom.*, **51**(5), 519-531.
- Yang, Z.J., Deeks, A.J. and Hao, H. (2007), “Transient dynamic fracture analysis using scaled boundary finite element method: A frequency-domain approach”, *Eng. Fract. Mech.*, **74**(5), 669-687.
- Yang, Z.J., Wang, X.F., Yin, D.S. and Zhang, C. (2015), “A non-matching finite element-scaled boundary finite element coupled method for linear elastic crack propagation modelling”, *Comput. Struct.*, **153**, 126-136.
- Yau, J.F., Wang, S.S. and Corten, H.T. (1980), “A mixed-mode crack analysis of isotropic solids using conservation laws of elasticity”, *J. Appl. Mech.*, **47**(2), 335-347.

CC